American Journal of Quantum Chemistry and Molecular Spectroscopy
2017; 1(1): 7-20
http://www.sciencepublishinggroup.com/j/ajqcms
doi: 10.11648/j.ajqcms.20170101.12

Adsorption on (Ni-H_2, Pd-H_2, Pt-H_2) Metal-Hydrogen Interaction: DFT Approach

Juan Manuel Larrea Munguía, Juan Horacio Pacheco Sánchez, Federico del Razo López

Division of Postgraduate Studies and Research, Technological Institute of Toluca, Metepec, México

Email address:
Jmlm_2011@hotmail.com (J. M. L. Munguía), jpachecos@toluca.tecnm.mx (J. H. P. Sánchez), fddelrazo@gmail.com (F. d. R. López)

To cite this article:
Juan Manuel Larrea Munguía, Juan Horacio Pacheco Sánchez, Federico del Razo López. Adsorption on (Ni-H_2, Pd-H_2, Pt-H_2) Metal-Hydrogen Interaction: DFT Approach. *American Journal of Quantum Chemistry and Molecular Spectroscopy*. Vol. 1, No. 1, 2017, pp. 7-20.
doi: 10.11648/j.ajqcms.20170101.12

Received: October 23, 2016; **Accepted**: December 26, 2016; **Published**: January 20, 2017

Abstract: Our aim is to find the kind of adsorption (physisorption or chemisorption) existent, where the interaction of one metal atom (Ni, Pd, Pt) with one hydrogen molecule is achieved for modeling potential energy surface using DFT approach. This molecular modeling is developed when attacking a metal atom with a hydrogen molecule. Attack starts at 10 Å considered as infinite distance for determining the energies step by step of 1 Å approaches of hydrogen to metal. The new metal–hydrogen molecule also called complex or intermediary is located at the minimum between the attractive and repulsive part of the potential energy curve of interaction. The adsorption energy and equilibrium distance corresponds to insert metal atoms in gas molecules. This study analyzes the interaction metal-hydrogen and compares with other researches. The metal-hydrogen interaction is at least useful in high-tech electronic materials, fuel cells, hydrogen batteries, and catalysis.

Keywords: Density Functional Theory, Potential Energy Curve, Adsorption, Physisorption Chemisorption

1. Introduction

Reaction mechanisms between transition metals of group VIII (Ni: ^{3}F, Pd: ^{1}S, and Pt: ^{3}D) and hydrogen molecule have been broadly investigated [1-30]. Nickel-hydrogen battery is a rechargeable electrochemical power source. Palladium has the potential to play a major role in many aspects of the hydrogen economy, including hydrogen purification, storage, detection, and fuel cells. The platinum catalyst and hydrogen fuel (H_2) have been widely applied to fuel cells. The aim in here is to build potential energy curves of metal-hydrogen interactions, in order to know mechanisms of hydrogen activation. Hydrogen lies in the form of water or organic compounds, and can be obtained from these sources. In order to separate it from its compounds, it must be supplied enough energy to reach the dissociation energy of the molecule. Transition metals play an important role in science, therefore it is vital the relationship between metal-hydrogen. Breaking of molecular hydrogen by transition metals is often to obtain the ionic hydrogen, which is of important use in electrical conductivity. It is applied as energy source in the case of fuel cells.

This modeling is carried out at level of density functional theory (DFT) of a molecular system. DFT has been established to calculate the energy as a functional of the molecular electron density, and represents an alternative to conventional ab initio methods in order to introduce the effects of electron correlation in the resolution of the system under study. According to DFT, the energy of the ground state of a many-electron system can be expressed from the electron density. Indeed, the use of electron density rather than the wave function for calculating energy, is the fundamental basis of DFT, which in fact calculates E_0 energy and other molecular properties from the electron density $_o$ of the ground state [31]. DFT was developed for electronic structures, organic or inorganic molecular properties, molecular crystals, covalent solids, metallic solids, and infinite surfaces [32]. DFT level of theory provides a computational alternative for determining the energy of atoms, molecules and solids [33-34]. The most fundamental DFT method is local density approximation (LDA), which assumes density behaves locally like a uniform electron gas. Generally this allows description of molecular properties [35]. One possibility going beyond the local density approximation in the context of DFT is the generalized gradient approximation (GGA) functional.

In a research conducted by Kunz *et al.* [20] the bonding curve for NiH is exhibited. They show $4s^2$ shell splits into

two sp hybrids. One is bonding orbital, which is doubly occupied using the H_{1s} electron, and the other one is non-bonding, and extends behind the Ni atom directly away from the NiH molecule. To see if this non-bonding orbital can bond another hydrogen atom, they constructed the corresponding pathway using unrestricted Hartree_Fock calculations. They found that this second hydrogen also forms a strong bond (2.2 eV) in a linear HNiH molecule at the minimum of the pathway. Guse *et al.* [27] calculated first the interaction Ni-H using symmetry $C_{\infty h}$ for linear molecules, and then they brought in a second hydrogen atom forming triplet H(NiH) also using linear symmetry. They consider that hydrogen interacts very weakly with the 3d electron, showing that the ground state of HNiH is derived from $3d^8 4s^2$ configuration of nickel. Using UHF-GVB methodology, they found 53.34 Kcal/mol and 1.64 Å as equilibrium point for H+NiH interaction. Recent results exhibit a similar energy coming from $^1S(d^{10})$ excited state [36].

Stability of PdH_2 molecule at ground state has been found by using ab initio calculations [15], and experimentally corroborated [16]. In matrix isolation experiments, from the infrared band structure, the existence of a stable Pd-H_2 complex with side-on structure (i.e., with C_{2v} symmetry) was conclusively inferred. For such structure, both hydrogen moieties are exactly equivalent when Pd and H_2 are in solid Xe matrices at 10-12 K deposited [16]. It was also observed infrared spectra of PdH_2 complex, and palladium hydrides in solid argon and neon, and calculated using DFT B3LYP functional [29, 30]. The interaction of hydrogen molecule with palladium is in the Pd-H_2 and Pd_2-H_2 systems studied as a model of chemisorption of one hydrogen molecule on a metal surface by Multi-Reference Symmetry Adapted Cluster expansion MR-SAC-CI [17]. The optimal path of the approach was calculated by the Hartree-Fock method for the Pd-H_2 system and by the CAS-MC-SCF method [18, 19].

One of the first *ab initio* theoretical studies with relativistic corrections and electronic correlation of the interaction of one hydrogen molecule with one platinum atom was developed by Poulain *et al.* [13, 37, 38]. They postulated that the singlet excited electronic state $^1S(d^{10})$ of Pt closed shell is responsible for H_2 capture. This state is correlated to the closed shell $^1A_1$ molecular state of the Pt-H_2 system. Poulain *et al.* [21] focused on *ab-initio* calculation for a potential energy curve of the hydrogen bond activation by transition metals. In a research using ab initio calculations Pacheco *et al.* [14] obtained a repulsive potential energy curve at the ground state, and a well of potential at the ^1S excited state of the Pt-H_2 interaction, which is an unexpected behavior in agreement with previous research [13, 21-24, 37, 38].

Using ab initio calculations with the coupled programs PSHONDO-IJKL-FOK-CIPSI in symmetry C_{nv}, a relative binding energy of -29.36 Kcal/mol was obtained at 3 (au) of distance for $5d^{10}$ (closed shell) state in Reference [11]. The same binding distance 3.00 (au) was obtained using the methodologies: DFT-B3LYO, MP2, and PSHONDO-IJKL-FOK-CIPSI; while binding energies -31.87 Kcal/mol (DFT-B3LYP), -32.55 (MP2) Kcal/mol and -29.36 Kcal/mol (PSHONDO-IJKL-FOK-CIPSI) are obtained [11]. The equilibrium potential among oxide-reductive reactions is 1.23 V [39]. Then, considering that the electrons are accelerated to this potential, the latter value corresponds to the energy of 28.37 Kcal/mol of the well-potential energy surface. Furthermore, Míšek [40] found 1.31 eV (30.21 Kcal/mol) as the formation energy of single vacancy in platinum, a value which was improved to 1.15 eV (26.523 Kcal/mol) by high pressure quenching experiments [25]. Jackson [41] found a value of 1.2 eV (27.68 Kcal/mol) for water quenches on single crystals of platinum. The source of disagreement between values of the formation energy for vacancies in platinum was also discussed by Emrick [25].

M. Alikhani and C. Minot [22] investigated the mechanism of the spontaneous activation of the hydrogen molecule (H_2) by a transition metal (Ni, Pd, Pt and Pd_2) using DFT-B3LYP by calculating the difference of energy between ^1S and ^3D states of the transition metals. They found results in good agreement with experiment.

In this study, potential energy surfaces (PES) of the metal hydrogen intermediary molecule by using GGA-PW91 and LDA-PWC functional are built: i) by bringing in the H_2 molecule in side on orientation to the metal atom (Ni, Pd and Pt) located at a fixed position, ii) by bringing in one H_2 molecule linearly in side on orientation to the target. This is in order to compare the equilibrium energy obtained against other research.

2. Methodology

A general flow chart of the methodology is exhibited in Figure 1.

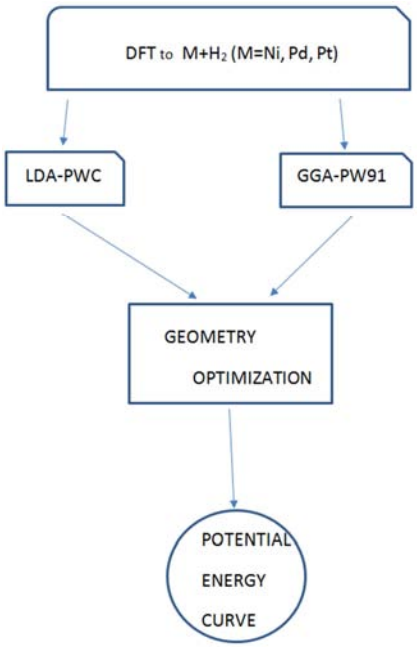

Figure 1. *Flow chart of the methodology.*

DFT energy calculations for transition metals (Ni, Pd, Pt)

with GGA-PW91 [42], and local density approximation LDA-PWC [43] were achieved using spin unrestricted, dnp basis sets, and O_h symmetry in order to compare with available results. Symmetry O_h for these systems provides the states ^2E_g HOMO, $^1A_{1g}$ LUMO when using LDA, and $^3T_{2g}$ HOMO, $^1A_{1g}$ LUMO when using GGA. Molecular behavior between a metal atom (Ni, Pd, Pt) and a hydrogen molecule (H_2) at DFT level of theory is achieved for electronic energy computations of metal-hydrogen interaction. Calculations with GGA-PW91 [42] and LDA-PWC [43] were accomplished through spin unrestricted and dnp basis sets. This study consists first in a geometry optimization of metal-hydrogen system, and then to build the whole potential energy curve. This modeling about head-on and side-on orientations for interactions in C_{4v} symmetry and C_{2v} symmetry) is carried on by approximations of the hydrogen molecule to the metal atom in these two orientations, in order to generate the corresponding intermediate molecule at the equilibrium point of the potential energy curve.

3. Results

First of all the optimized geometry of one hydrogen molecule provides the equilibrium point at r_e=0.748Å and E_e=-100.171 kcal/mol using DFT-GGA-PW91 functional, and r_e=0.764Å and E_e=-108.713 kcal/mol using DFT-LDA-PWC functional. The experimental result is E_{exp} = 103.257 kcal/mol and r_{exp} = 0.741 Å [44]. The optimization closer to the experimental result was obtained using GGA functional.

DFT energy magnitudes for transition metals of group VIII: Ni, Pd and Pt at the ground state are given in Table 1. All of these results were expected to be near cero. Experimental energy at the ground state ^1S is only comparable with palladium as observed in Table 1, and the DFT energy value of Ni and Pt are closer to the experimental ^1D excited state, despite that the ground state of Nickel is ^3F, Palladium ^1S and Platinum ^3D.

Table 1. *Energy in [Kcal/mol] obtained by DFT method.*

Transition metal	LDA-PWC	HOMO-LUMO	GGA-PW91	HOMO-LUMO	State
	|E|		|E|		$\|E_{exp}\|$
Ni	30.356	29-30	29.18	29-30	^1D: 38.65
Pd	1.796	46-47	1.038	46-47	^1S: 0
Pt	44.437	78-79	29.243	78-79	^1D: 17.55

Table 2. *Equilibrium energy and distance obtained by geometry optimization for these metal-hydrogen interactions. Energy in Kcal/mol, and distance in Angstroms [Å].*

Interaction	Functional	Orientation	E_{eq}	r_{eq}	HOMO-LUMO	Symmetry state
Ni-H_2	GGA	Side-on	-168.214	1.463	30-31	A_1/B_1
		Head-on	-156.106	2.773	29-30	A_1/A_1
	LDA	Side-on	-187.814	1.442	30-31	A_1/B_1
		Head-on	-166.162	1.998	30-31	A_1/B_1
Pd-H_2	GGA	Side-on	-122.335	1.811	48-49	A_1/A_1
		Head-on	-133.472	1.724	48-49	B_1/A_1
	LDA	Side-on	-111.649	1.872	48-49	A_1/A_1
		Head-on	-123.327	1.775	48-49	B_1/A_1
Pt-H_2	GGA	Side-on	-142.759	1.906	80-81	A_1/A_1
		Head-on	-138.816	1.998	80-81	B_2/A_1
	LDA	Side-on	-176.690	1.808	80-81	A_1/A_1
		Head-on	-168.28	1.826	80-81	B_1/A_1

The equilibrium energy and distance after the geometry optimization of these transition metals are given in Table 2, within the corresponding symmetry and HOMO-LUMO numbers associated to the metal as acid (acceptor) receiving an electron pair in its lowest unoccupied molecular orbital (LUMO) from the highest occupied molecular orbital (HOMO) of a base (donor) gas. The HOMO from the base and the LUMO from the acid combine with a bonding molecular orbital. This equilibrium point is not enough to know the size of the bond strength, which is the same than the well of potential size, useful to know the dissociation energy, and the possible adsorption type among reactants.

Therefore, the construction of the potential energy curve is vital to obtain such information. In order to get this, the corresponding relative energies calculated were translated to the origin as shown in graphs of Figures 2, 3 and 4 with the aim to obtain directly the potential well depth; these Figures also exhibit the cartoon of the input of the system, where the hydrogen molecule has been optimized. The corresponding interactions are: Ni-H_2, Pd-H_2, and Pt-H_2, in Figures 2, 3, 4 respectively. Dash and dot curves correspond to head-on reaction, and their very small potential well depth correspond to physisorption in Figure 2, while continuous and short dash curves with high potential well depth correspond to chemisorption according to Atkins ranges [45]. The only dot curve at head-on reaction clearly corresponds to physisorption in Figure 3, continuous and dash dot curves are not easy to classify according to Atkins ranges, while dash curve clearly correspond to chemisorption. In Figure 4 again it is easy to classify dot and dash curves as physisorption and chemisorption respectively, because these are the smallest and the highest well depths; and the continuous, and dash dot curves are neither easy to classify. The expected type of adsorption is physisorption for M+HH linear head-on

reactions, and chemisorption for M+H_2 non-linear side-on reactions.

The potential energy curves between the metal atoms (Ni, Pd and Pt) and molecular hydrogen H_2 were obtained by GGA and LDA functional for comparison, using head-on and side-on orientations at the interaction as shown in Figures 2, 3, 4. In Figure 2 using GGA-PW91 functional, potential energy curves have been built in two orientations: i) in side-on orientation, the equilibrium point is located at energy 124.237 kcal/mol and distance 1.0 Å, at the minimum of the well of potential, ii) head-on orientation lead us to the equilibrium point located at energy 4.982 kcal/mol and distance 2.773 Å. Using LDA-PWC functional potential energy curves are: i) side-on orientation take us to the equilibrium point 125.477 kcal/mol and 1.998 Å, and ii) head-on orientation lead us to an energy 5.524 kcal/mol and a distance of 1.998 Å at the minimum of the well of potential.

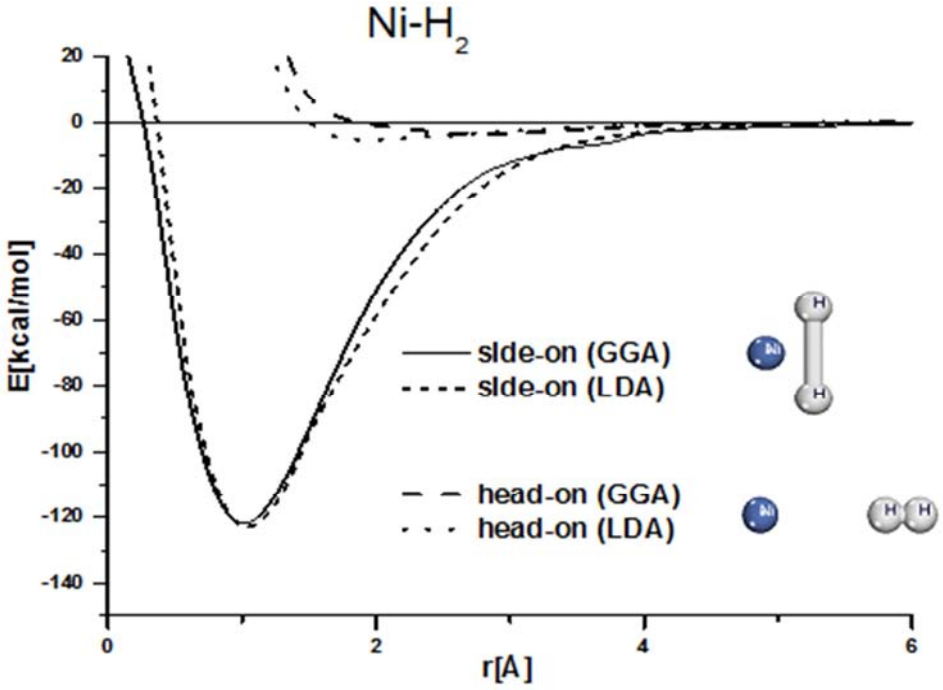

Figure 2. *Relative energy as a function of the distance between Ni and H_2 in side-on reaction, and Ni and the closest H atom in H_2 in head-on reaction.*

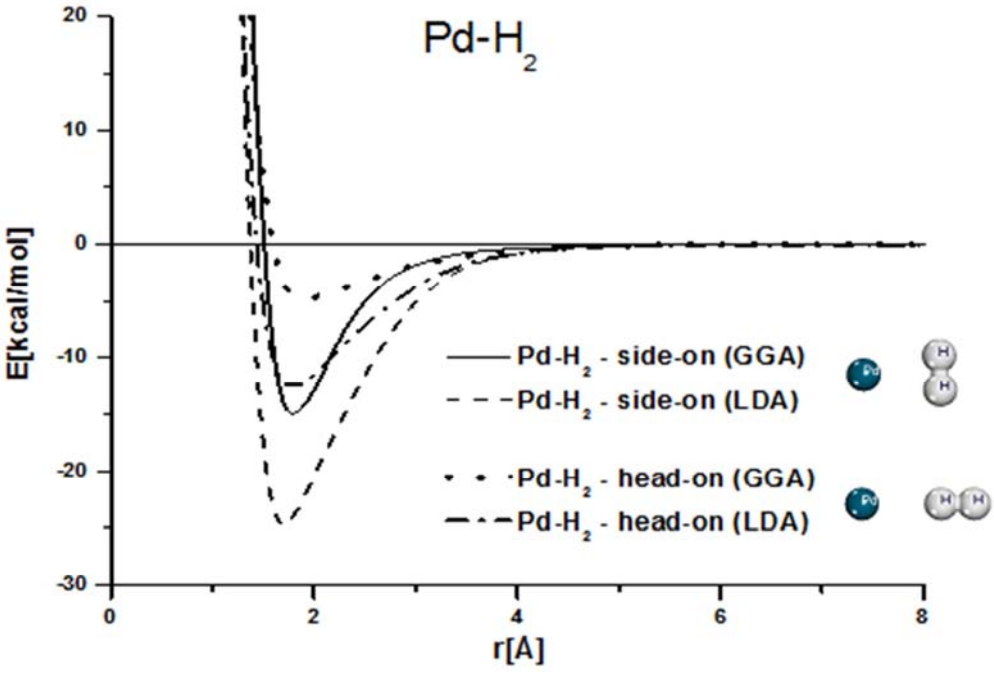

Figure 3. *Potential energy curves for Pd-H_2 interaction have been calculated by DFT using LDA and GGA functional when moving the hydrogen molecule in both side-on and head-on.*

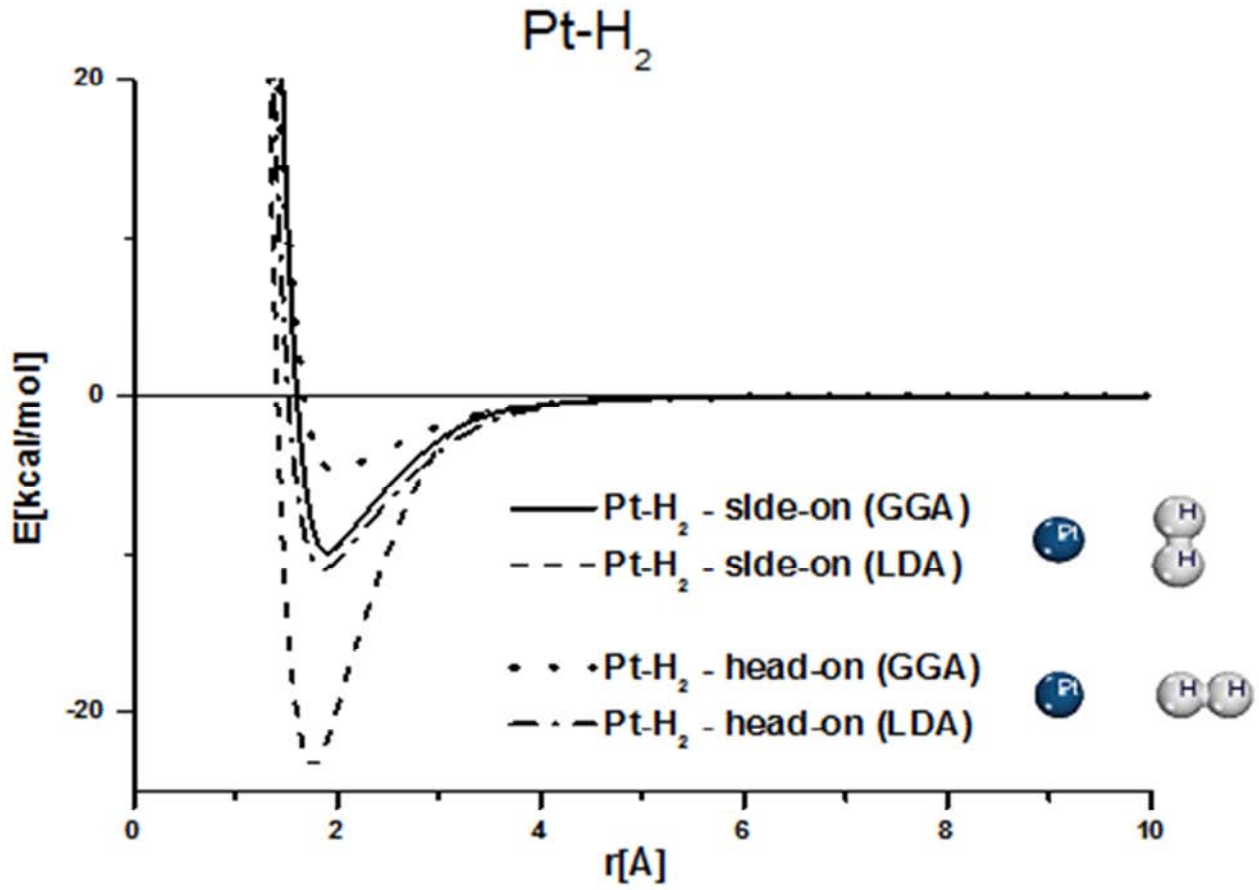

Figure 4. *Potential energy curves of Pt-H_2 interaction in side-on and head-on orientations. These were step by step calculated using DFT (GGA and LDA) level of theory.*

In Figure 3, using GGA-PW91 functional, potential energy curves have been built in two orientations: i) in side-on, the equilibrium point is located at energy 14.92 kcal/mol and distance 1.75 Å, at the minimum of the well of potential, ii) head-on orientation lead us to the equilibrium point located at energy 5.52 kcal/mol and distance 1.97 Å. Using LDA-PWC functional potential energy curves are: i) side-on orientation take us to the equilibrium point 26.29 kcal/mol and 1.66 Å, and ii) head-on orientation lead us to an energy 13.46 kcal/mol and a distance of 1.77 Å as potential well depth.

In Figure 4, using GGA-PW91 functional, potential energy curves have been built in two orientations: i) while in side-on the equilibrium point is located at energy 10.706 kcal/mol and distance 1.860 Å, at the minimum of the well of potential, ii) head-on orientation lead us to the equilibrium point located at energy 5.165 kcal/mol and distance 1.998 Å. Using LDA-PWC functional potential energy curves are: i) side-on orientation take us to the equilibrium point 23.573 kcal/mol and 1.753 Å, and ii) head-on orientation lead us to an energy 11.625 kcal / mol and a distance of 1.826 Å at the minimum of the well of potential.

Comparisons of equilibrium points of our results have been achieved against other researches, and shown in Tables 3 and 4 for side-on and head-on orientations, respectively. Table 3 shows the calculated equilibrium points side-on orientation calculated by DFT method, and compared with other investigations. Linear calculations of H+NiH lead to HNiH complexes [12, 20, 27] which are compared as side-on by us. When a DFT is used: i) Ni-H_2 equilibrium energy agrees with a semiempirical SCF result of 1^3A_1 state reported by Ruette *et al*. [26]; however it does not agree with the ab initio unrestricted Hartree_Fock calculations found by Kunz *et al*. [20], neither with the semiempirical SCF result of the 1^1A_1 state reported by Ruette *et al*. [26]. ii) Pd-H_2 equilibrium energy GGA-PW91 agrees with Jarque *et al*. study [15]. This comparison is among GGA-PW91 and ab initio calculations. iii) Pt-H_2 equilibrium energy obtained by GGA-PW91 do not agree with that reported by Pacheco *et al*. [14]; however the equilibrium energy calculated by LDA-PWC agrees with Pacheco *et al*. [14] research. There is a significant problem in the latter comparison, because it is between the ground state calculated by LDA-PWC, and a first excited state ($^1S:5d^{10}$) obtained by means of ab initio calculations. Alikhani and Minot [22] research using DFT-B3LYP does not represent any comparison on equilibrium energy with our metal–hydrogen interactions. Table 4 exhibits the equilibrium point of metal-hydrogen interaction at the minimum of the potential energy curve: i) In case of Pt-H_2 our equilibrium energy is not close to that reported by Poulain *et al*. [21]. ii) In case of Pd-H_2 there is no equilibrium energy comparable to that reported by Jarque *et al*. [15]. iii) In case of Ni-H_2 we made an inference.

Table 3. *Side-on orientation for comparison among our calculations and other researches were accomplished. Energy in kcal/mol, and distance in angstroms.*

Interaction	GGA-PW91		LDA-PWC		Other Researches	
	E_{eq}	r_{eq}	E_{eq}	r_{eq}	E_{eq}	r_{eq}
Ni-H_2	124.23	1.0	125.47	1.99	63.53[12]	1.537[12]
					50.739[20]	1.79[20]
					~37.0[22]	1.42[22]
					53.0[26]	1.82[26]
					124.13[26]	1.47[26]
					53.34[27]	1.64[27]
Pd-H_2	14.92	1.75	26.29	1.66	14.0[15]	1.78[15]
					~15.0[17]	1.65[17]
					13.0[22]	1.51[22]
					18.0[22]	1.85[22]
					18.0[29]	1.698[29]
					17.5[30]	1.517[30]
Pt-H_2	10.70	1.86	23.57	1.75	50.0[22]	1.52[22]
					25.03[9]	1.56[9]
					~26.0[23]	1.55[23]
					26.52[25]	----

Table 4. *Head-on orientation for comparison among our equilibrium energy and other researches were accomplished. Energy in kcal/mol and distance in angstroms.*

Interaction	GGA		LDA		Other Researches	
	E_{eq}	r_{eq}	E_{eq}	r_{eq}	E_{eq}	r_{eq}
Ni-H_2	4.98	2.77	5.52	1.99	----	----
Pd-H_2	5.52	1.87	13.46	1.77	10.0[15]	2.23[15]
Pt-H_2	5.16	1.99	11.62	1.82	~3.7[21]	1.69[21]

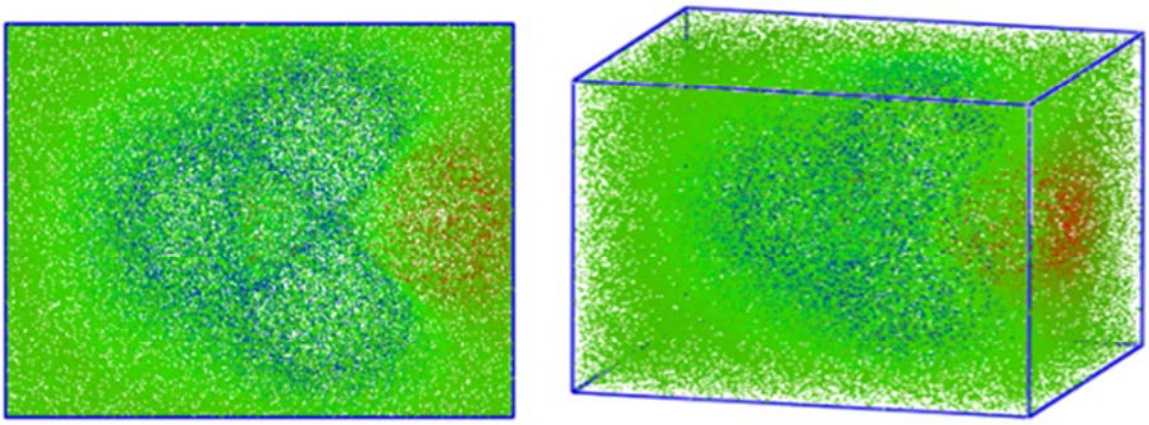

Figure 5. *DFT-GGA. Hybrid orbital of Pt-H_2 interaction in side on orientation (HOMO).*

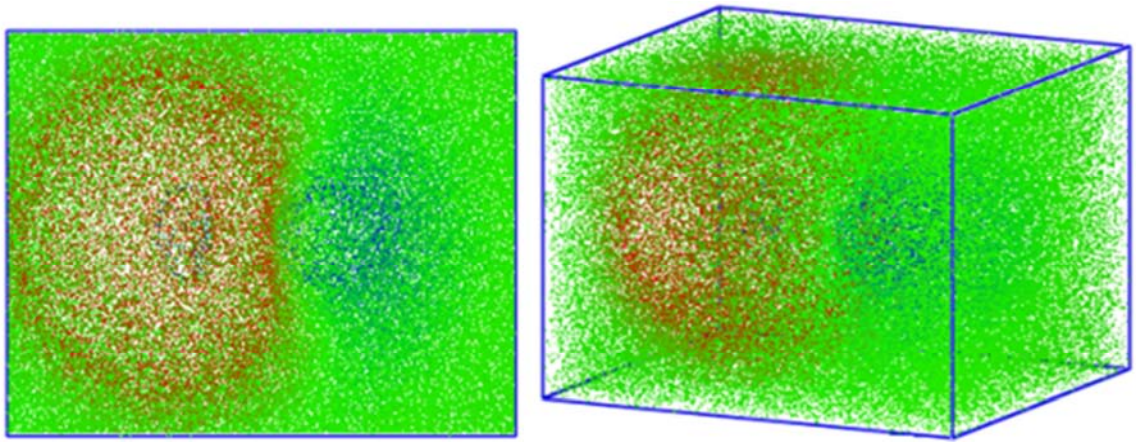

Figure 6. *DFT-GGA. Hybrid orbital of Pt-H_2 interaction in side on orientation (LUMO).*

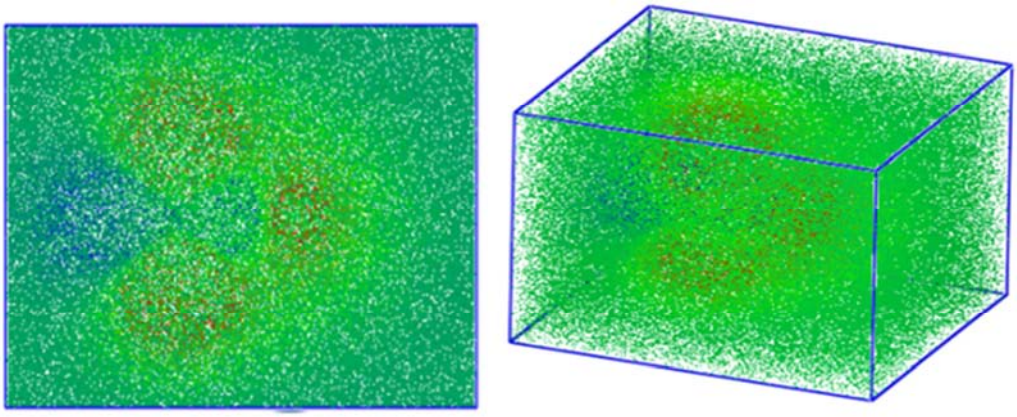

Figure 7. *DFT-GGA. Hybrid orbital of Pd-H_2 interaction in side on orientation (HOMO).*

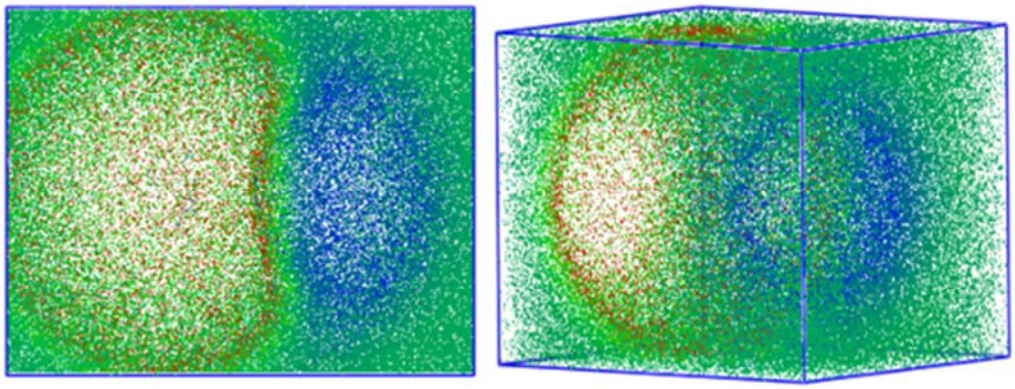

Figure 8. *DFT-GGA. Hybrid orbital of Pd-H_2 interaction in side on orientation (LUMO).*

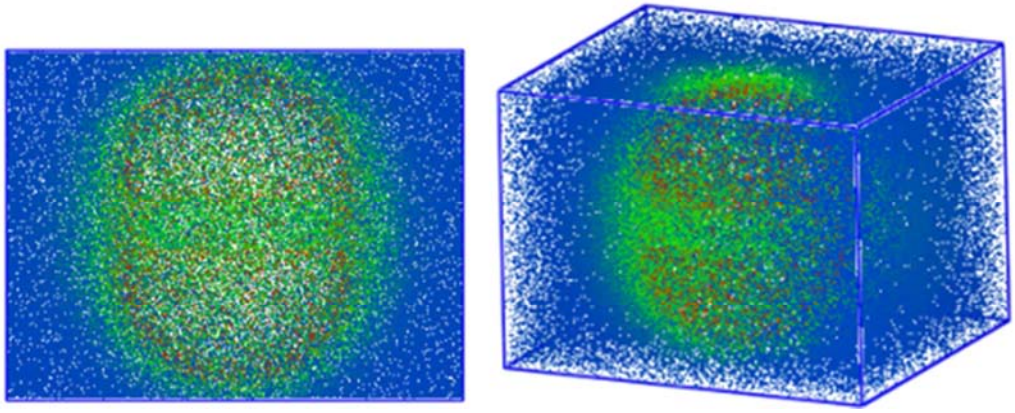

Figure 9. *DFT-GGA. Hybrid orbital of Ni-H_2 interaction in side on orientation (HOMO).*

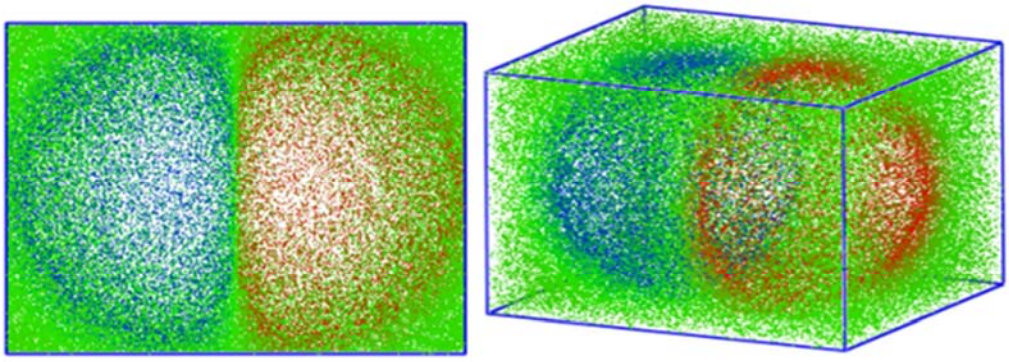

Figure 10. *DFT-GGA. Hybrid orbital of Ni-H_2 interaction in side on orientation (LUMO).*

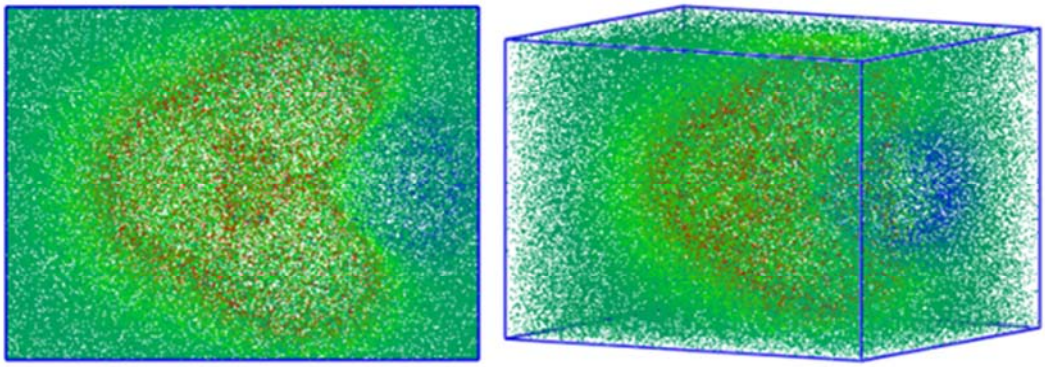

Figure 11. *DFT-LDA. Hybrid orbital of Pt-H_2 interaction in side on orientation (HOMO).*

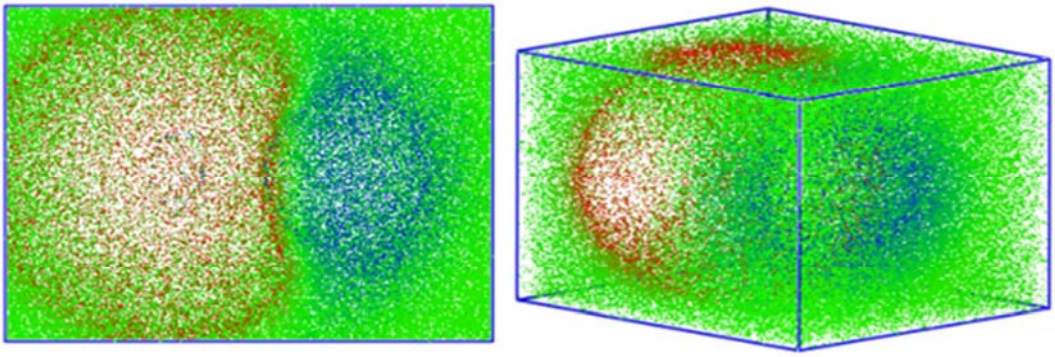

Figure 12. *DFT-LDA. Hybrid orbital of Pt-H_2 interaction in side on orientation (LUMO).*

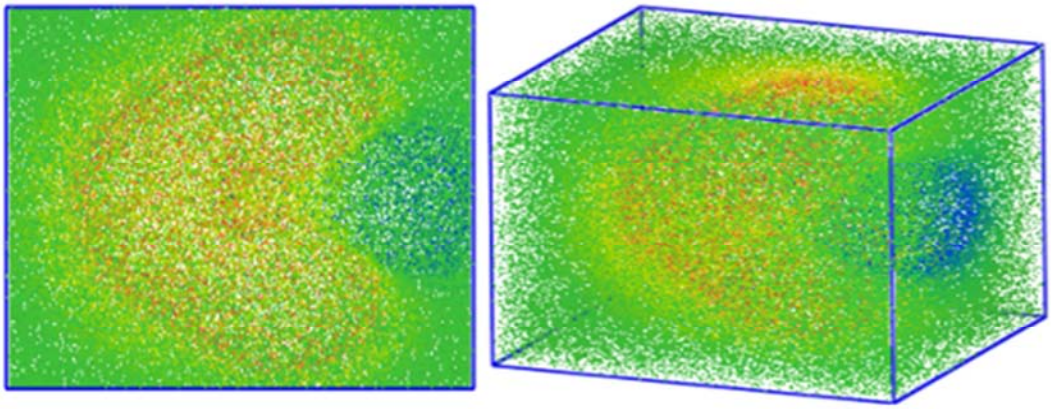

Figure 13. *DFT-LDA. Hybrid orbital of Pd-H_2 interaction in side on orientation (HOMO).*

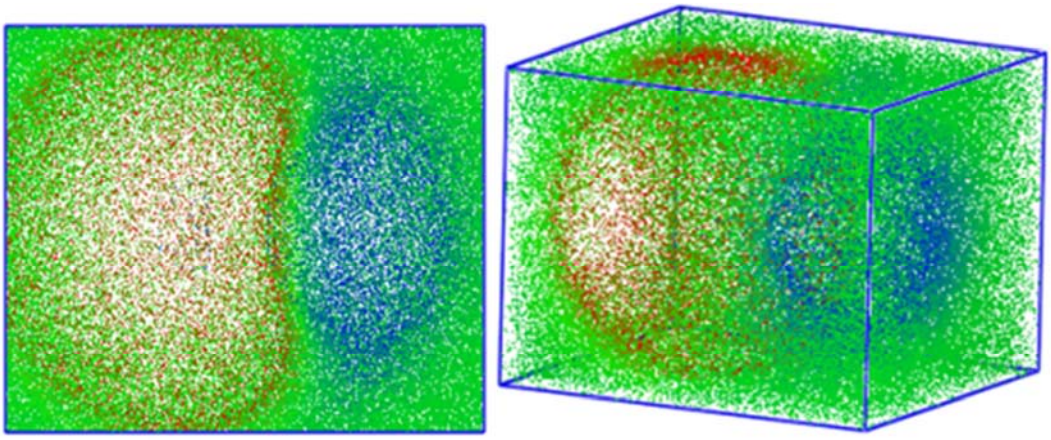

Figure 14. *DFT-LDA. Hybrid orbital of Pd-H_2 interaction in side on orientation (LUMO).*

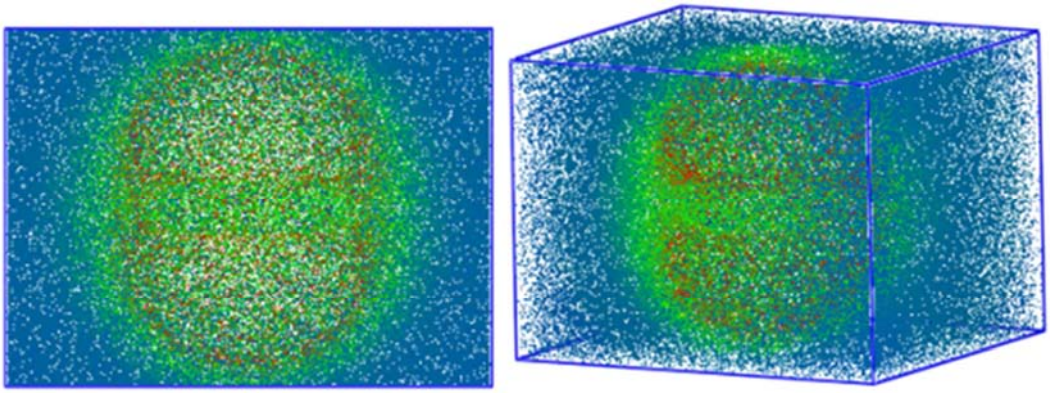

Figure 15. *DFT-LDA. Hybrid orbital of Ni-H_2 interaction in side on orientation (HOMO).*

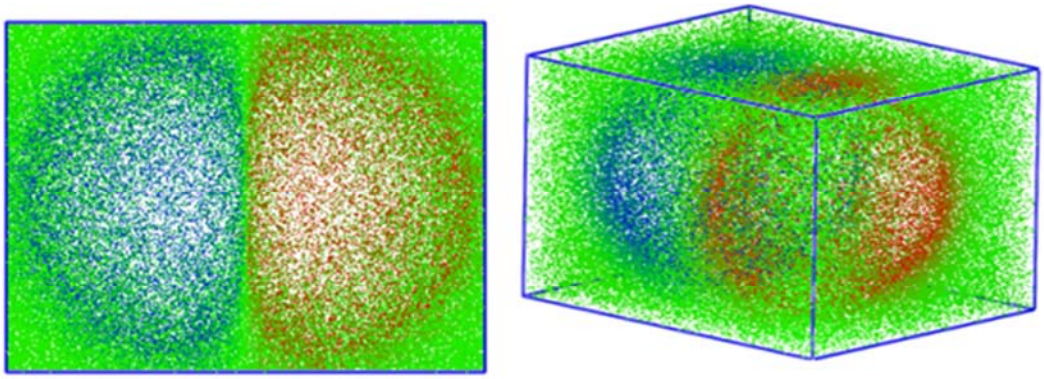

Figure 16. *DFT-LDA. Hybrid orbital of Ni-H_2 interaction in side on orientation (LUMO).*

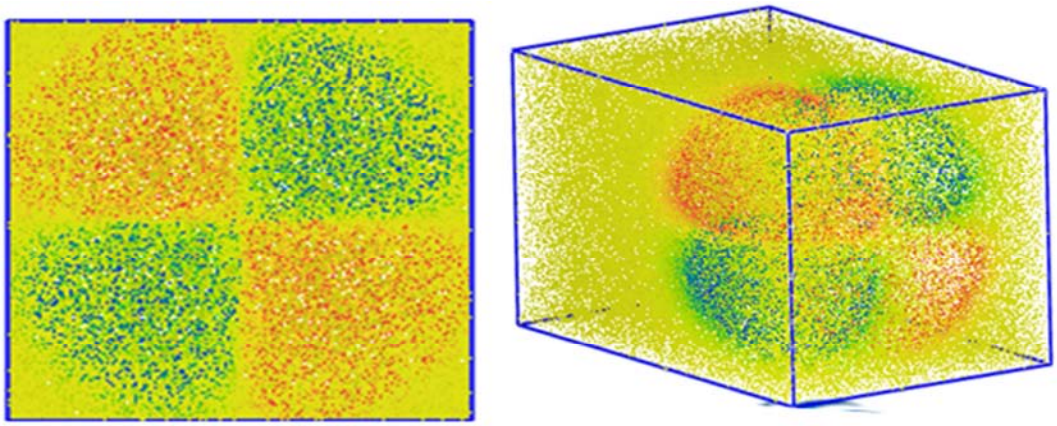

Figure 17. *DFT-GGA. Hybrid orbital of Pt-H_2 interaction in head on orientation (HOMO).*

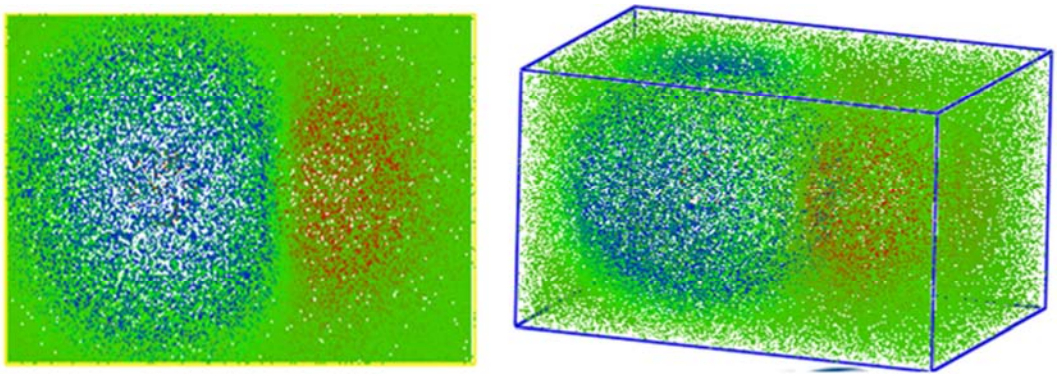

Figure 18. *DFT-GGA. Hybrid orbital of Pt-H_2 interaction in head on orientation (LUMO).*

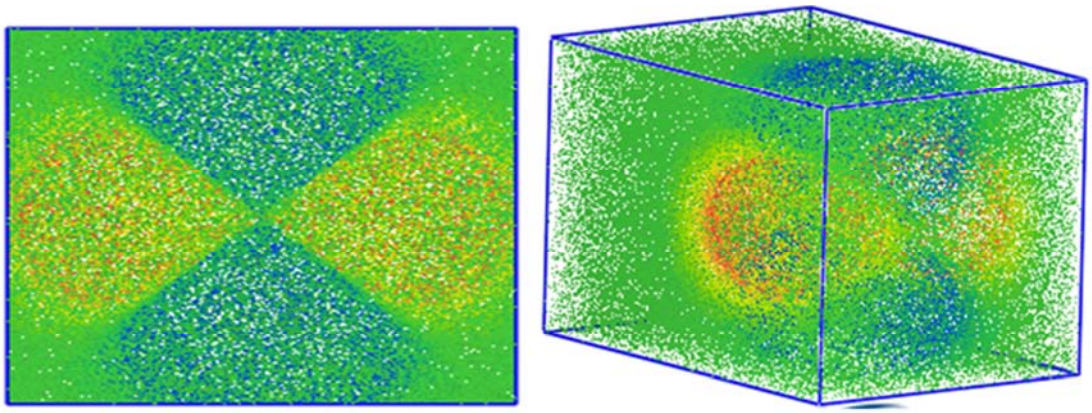

Figure 19. *DFT-GGA. Hybrid orbital of Pd-H_2 interaction in head on orientation (HOMO).*

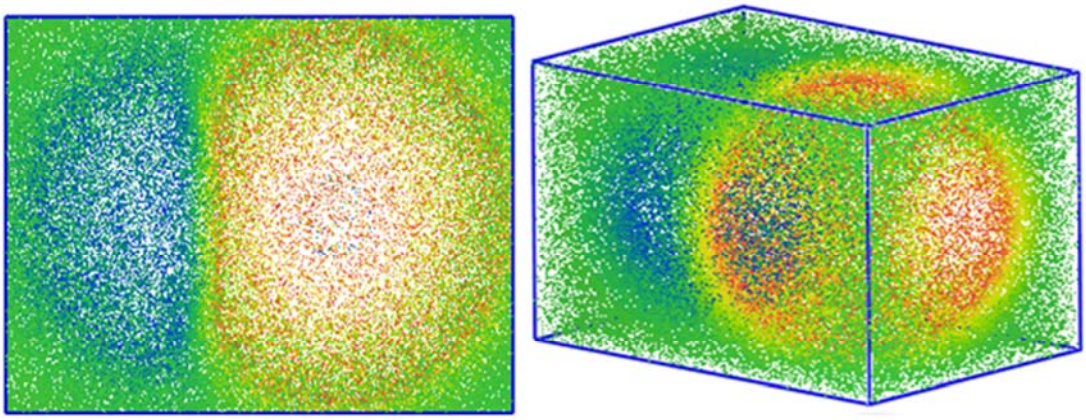

Figure 20. *DFT-GGA. Hybrid orbital of Pd-H_2 interaction in head on orientation (LUMO).*

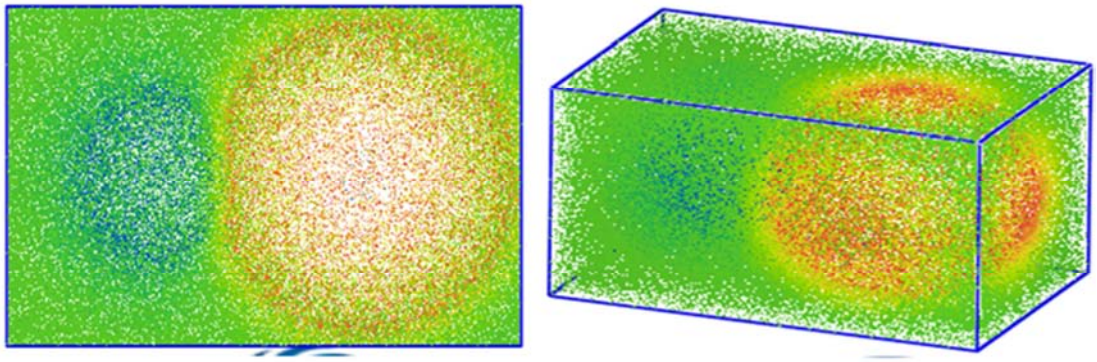

Figure 21. *DFT-GGA. Hybrid orbital of Ni-H_2 interaction in head on orientation (HOMO).*

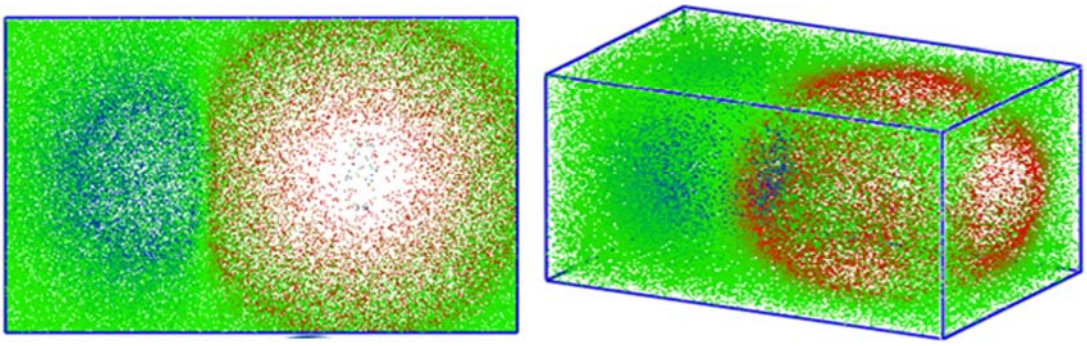

Figure 22. *DFT-GGA. Hybrid orbital of Ni-H_2 interaction in head on orientation (LUMO).*

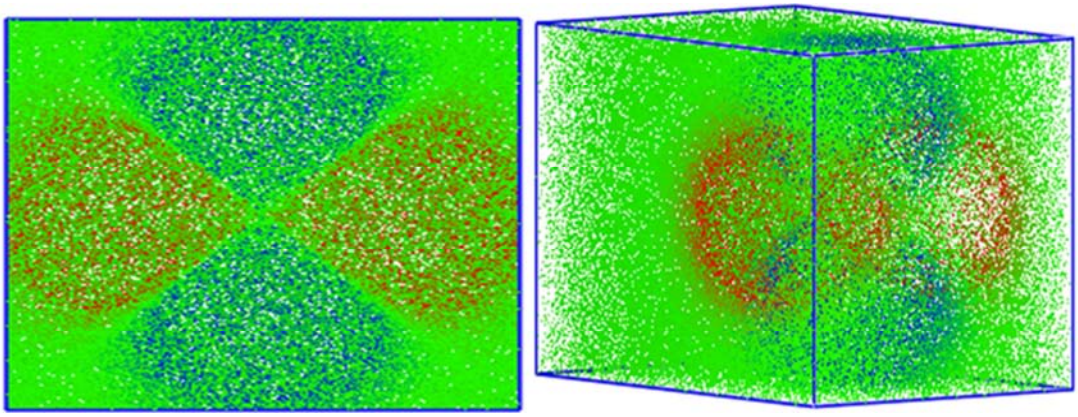

Figure 23. *DFT-LDA. Hybrid orbital of Pt-H_2 interaction in head on orientation (HOMO).*

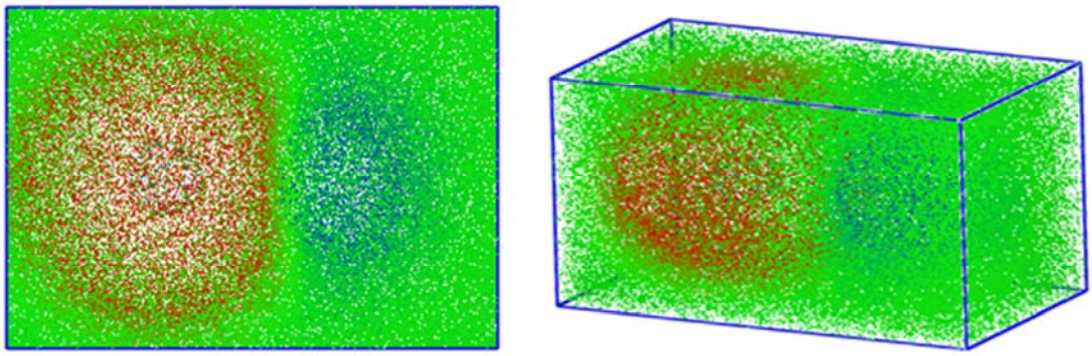

Figure 24. *DFT-LDA. Hybrid orbital of Pt-H_2 interaction in head on orientation (LUMO).*

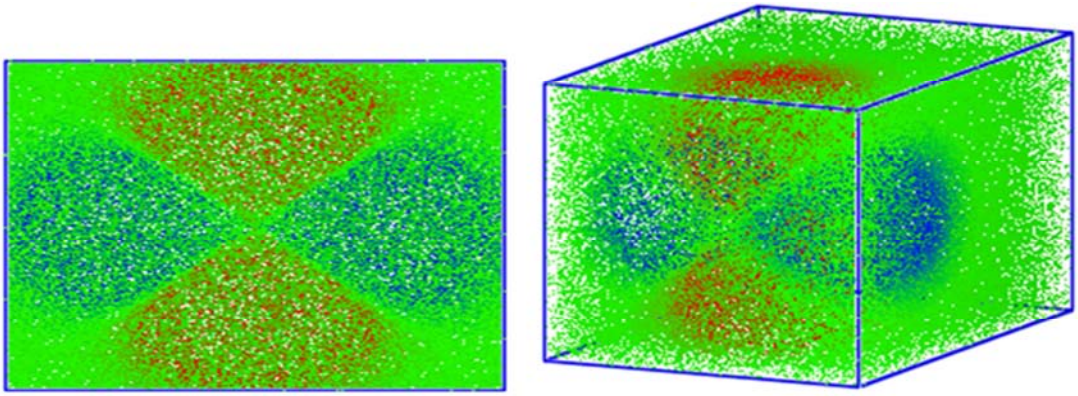

Figure 25. *DFT-LDA. Hybrid orbital of Pd-H_2 interaction in head on orientation (HOMO).*

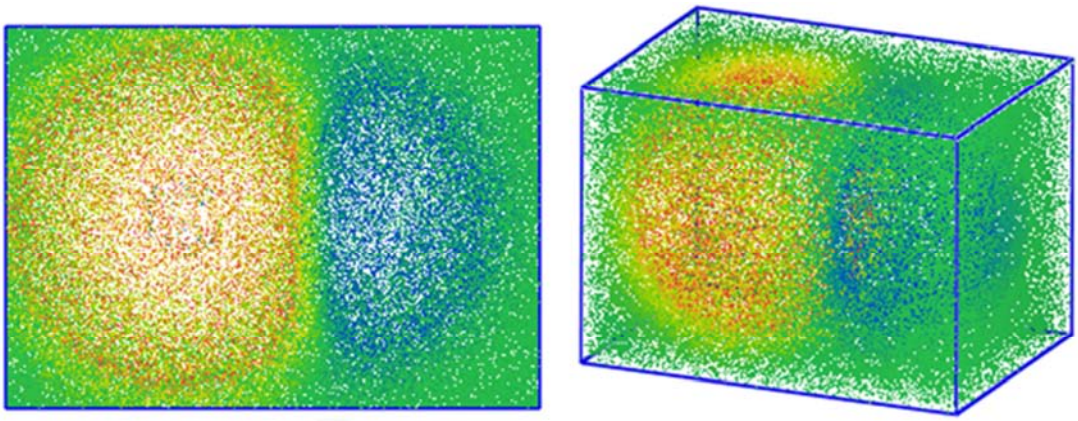

Figure 26. *DFT-LDA. Hybrid orbital of Pd-H_2 interaction in head on orientation (LUMO).*

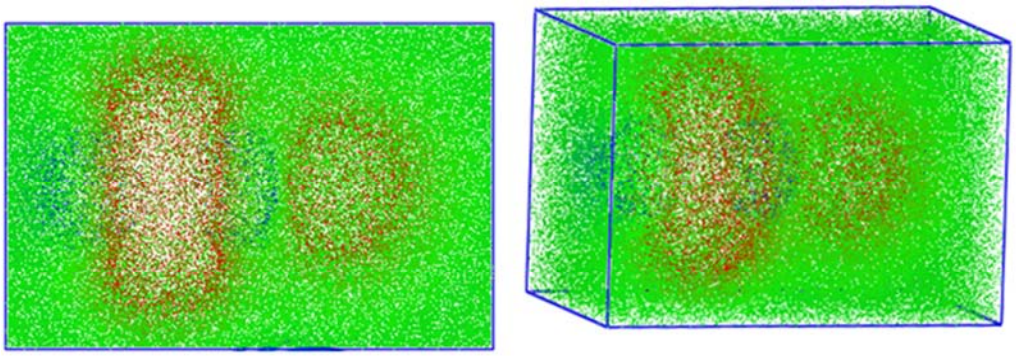

Figure 27. *DFT-LDA. Hybrid orbital of Ni-H_2 interaction in head on orientation (HOMO).*

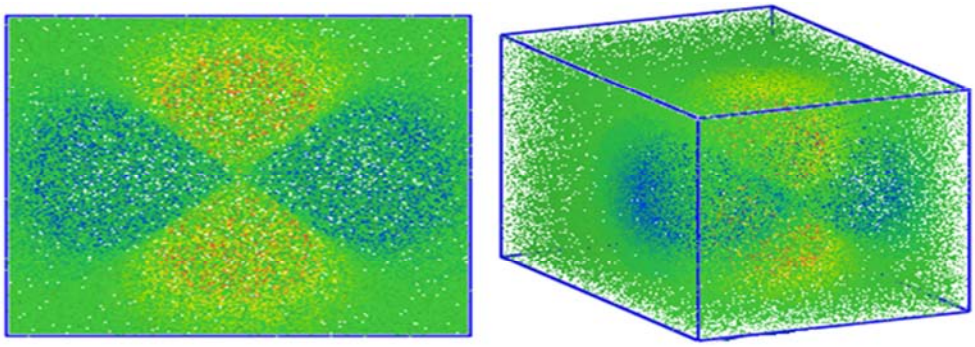

Figure 28. *DFT-LDA. Hybrid orbital of Ni-H_2 interaction in head on orientation (LUMO).*

Figures 5 to 28 correspond to every orbital HOMO-LUMO considered. Each Figure is observed in two different orientations of the same Figure. We have 24 Figures for only 12 potential energy curves because these are two perspectives: 12 for HOMO, and 12 for LUMO. Considering that metals have four HOMO-LUMO lobes, the action of hydrogen on metals is observed by the deformation of such lobes in Figures 2, and 4 when GGA functional is applied, and in Figures 8, and 10 when LDA functional is applied. However, it is observed lobes swelling in Figures 14, and 16 when GGA functional is applied, and in Figures 20, 22 and 25 when LDA functional is applied. Nickel case present different HOMO-LUMO orbitals than Pt and Pd as shown in Figures 6 and 18 when GGA functionals are applied; and also in Figures 12 and 24 when LDA is applied. In the whole Figures Nickel present different HOMO-LUMO orbitals than Platinum and Palladium. The later metals exhibit certain similarity in their HOMO-LUMO orbitals.

4. Discussion

In these three metal-gas equilibrium energies of the ground state we have: i) our calculations of Ni-H_2 DFT agree with the 1^3A_1 excited state reported at HNiH angle of 175° by Ruette *et al*. [26], which is almost linear. Their calculations were accomplished in C_{2v} symmetry considering the HNiH angle as reaction coordinate at a fixed distance among H and NiH. ii) Pd-H_2 calculated using DFT-GGA-PW91 agrees with those calculated by means of *ab initio* calculations [15, 17]. It was expected due to calculations are side-on for the ground state in both cases. iii) Interaction Pt-H_2 calculated using DFT-LDA-PWC agrees with Pt-H_2 (first excited state of Pt) obtained by means of *ab initio* calculations [14, 23, 24], and also with the quenching experimental value measured by Emrick [25]. Then, another unexpected result is a comparison between DFT-ground state, and *ab initio* first excited state. These facts lead us to assume that DFT calculates only the deepest well of potential among the different states of the interaction.

Observations of hydrogen adsorption on platinum through the work function and its removal by bombardment of positive-ions from the platinum surface in order to clean it were achieved long time ago [46]. Another way to test adsorption of hydrogen on platinum was by the change of platinum resistance under hydrogen action [47]. Actually, there are norms as ASTM 2006: D3908-03 to measure hydrogen chemisorption on platinum [10]. Furthermore, there are ranges to handle physisorption or chemisorption as enthalpy around 20 KJ/mol or 200 KJ/mol [45], respectively. Then, in our case, four cases of head-on reactions correspond to physisorption: three GGA cases and one LDA case (Ni-H_2). Therefore, physisorption occurs at head-on reactions, and chemisorption occurs at side-on reactions according to the rest of the calculations.

The reaction products M + H_2 are transition metal atoms (M = Ni, Pd, Pt) and molecular hydrogen (H_2). In our calculations, the complex is HMH in side-on orientation and MHH in head-on orientation. The breaking of this complex leads to products H + MH. Physisorption in the complex MHH leads to hydrogen formation easier than chemisorption in the complex HMH. These metal catalysts break hydrogen molecules mostly when these arrive in

head-on orientation to the metal supported in activated carbons, due to the physisorption behavior of MH_2 interaction. Then, most of the hydrogen in fuel cells comes from physisorption after the metal-hydrogen reaction in the anion of a fuel cell.

5. Conclusions

In these three cases, there is insertion of the metal in the hydrogen gas according to the corresponding wells of potential. GGA calculations on head-on orientation are always physisorption, while in side-on orientation chemisorption is truly reached according to the literature. In our three cases, side-on insertion is non-linear HMH (M = Ni, Pd, Pt), and head-on insertion is linear MHH.

In our DFT calculations of Ni-H_2 in side-on orientation the equilibrium energy agree with Ruette *et al*. [26] results for HMH linear insertion. The side-on orientation of Pd-H_2 GGA-PW91 result is comparable with most of the results shown in Table 3. The result in side-on orientation of Pt-H_2 LDA-PWC has an energy value comparable to the quenching experimental value 26.52 Kcal/mol (1.15 eV) measured by Emrick. Palladium and Platinum insert the hydrogen molecule in non-linear geometry. Then, the equilibrium energy of the interaction Pt-H_2 was found between oxide and reductive reactions, which represents a bridge bond between the theoretical calculations and the processes of transformation of the fuel in the Full Cells

Our DFT equilibrium energy prediction of Ni-H_2 in head-on orientation was not compared because in case of NiHH we did not find any result previously reported. The equilibrium energy in head-on orientation for PdHH is nearby in accordance with Jarque *et al* [15] in both GGA and LDA functionals. Finally the equilibrium energy in head-on orientation of PtHH GGA-PWC agrees with Poulain *et al.* [21] calculations.

These results indicate that taking care of the functional selected, DFT level of theory not only can be applied on large but also on small systems.

Acknowledgements

This research was financially supported by DGEST 5164.13-P grant.

References

[1] H. Nakatsuji and M. Hada, *Croat. Chim. Acta* 57 (1984) 1371.

[2] K. Balasubramanian, *Chem. Phys. Lett.* 135 (1987) 288.

[3] M. R. A. Blomberg, P. E. M. Siegbahn and B. O. Roos, *Mol. Phys.* 47 (1982) 127.

[4] M. R. A. Blomberg and P. E. M. Siegbahn, *J. Chem. Phys.* 78, (1983) 5682.

[5] M. R. A. Blomberg, U. Brandemark, L. Pettersson and P. E. M. Siegbahn, Int. J. of Quantum Chem., 23, (1983) 855-863

[6] S. Li, R. J. Van Zee, W. Weltner Jr., M. G. Cory and M. C. Zerner *J. Chem. Phys.* 106, (1997) 2055.

[7] M. E. Geusic, M. D. Morse, and R. E. Smalley, *J. Chem. Phys.* 82 (1985) 590.

[8] J. J. Low and W. A. Goddard III, *J. Am. Chem. Soc.* 106 (1984) 8321.

[9] X. Liu *et al.*, *J Phys Chem B Condens Matter Mater Surf Interfaces Biophys.* 110 (2006) 2013.

[10] ASTM 2006: D3908-03 Standard Test Method for Hydrogen Chemisorption on Supported Platinum on Alumina Catalysts and Catalyst Carriers by Volumetric Vacuum Method.

[11] J. H. Pacheco I. P. Zaragoza, L. A. García, and A. Bravo *Rev. Mex. Fís.* 52 (2006) 172.

[12] P. Jena, S. N. Khanna, and B. K. Rao "Clusters and Cluster Reactions" in *Density Functional Theory of Molecules, Clusters, and Solids. Edited by D. E. Ellis.* Kluwer Academic Publishers. Dordrecht, Netherlands (1995).

[13] E. Poulain, J. García-Prieto, M. E. Ruiz, and O. Novaro, *Int. J. Quantum Chem.* 29 (1986) 1181.

[14] J. H. Pacheco and A. Bravo, O. Novaro. Revista Mexicana de Fisica 52 (2006) 395.

[15] C. Jarque and O. Novaro, M. E. Ruiz, and J. Garcia-Prieto, J. Am. Chem, Soc.1986, 108, 3507.

[16] G. A. Ozín and J. García-Prieto, *J. Am. Chem. Soc.* 1986, *108,* 3099.

[17] H. Nakatsuji and M. Hada in *Applied Quantum Chemistry* edited by V. H. Smith, H. F. Schaefer, and K. Morokum. (1986). D. Reidel Publishing Company, Dordrecht, Holland. pp. 102-104.

[18] B. Roos, P. Taylor, and P. Siegbahn, Chern. Phys. 48, 157 (1980).

[19] P. Siegbahn, A. Heiberg, B. Roos, and B. Levy, Phys. Scripta, 21, 323 (1980).

[20] A. B. Kunz, M. P. Guse, and R. J. Blint, Chem. Phys. Lett. 37(3), 512 (1976).

[21] E. Poulain, F. Colmenares, S. Castillo and O. Novaro. Journal of Molecular Structure (Theochem). 210 (1990) 337-351.

[22] M. E. Alikhani and C. Minot. J. Phys. Chem. A 2003, 107, 5352-5355.

[23] K. Balasubramanian, J. Chem. Phys., 87 (1987) 2800.

[24] H. Nakatsuji, Y. Matsuzaki and T. Yonezawa, J. Chem. Phys., 88 (1988) 5759.

[25] R. M. Emrick, *Journal of Physiscs F: Met Phys.* 12 (1982) 1327.

[26] F. Ruette, G. Blyholder, and Head, J. Chem. Phys. 80, 2042 (1984).

[27] M. P. Guse, R. J. Blint, A. B. Kunz, *Int. J. Quantum Chem.* 11 (1977) 725 M.

[28] E. K. Parks, K. Liu, S. C. Richtsmeier, I. G. Pobo, and S. J. Riley, J. Chem. Phys. 82, (1985) 5470-5474.

[29] L. Andrews, Chem. Soc. Rev. 33 (2004) 123.

[30] L. Andrews, X. Wang, M. E. Alikhani, and L. Manceron, *J. Phys. Chem. A* 105 (2001) 3052.

[31] Ira N. Levine. (2001). *Quantum Chemistry*. Prentice Hall, NJ 2000.

[32] B. Delley, J. Chem. Phys. 1990, 92, 508; J. Chem. Phys. 1991, 94, 7245; J. Chem. Phys. 2000, 7756; J. Phys. Chem. 1996, 100, 6107.

[33] R. G. Parr, W. Yang. (1989). *Density Functional Theory of Atoms and Molecules*. Oxford University Press, Oxford.

[34] R. M. Dreizler, E. K. U. Gross. (1990). *Density Functional Theory-an Approach to the Quantum Many- Body Problem*. Springer. Berlin.

[35] John P. Lowe, Kirk A. Peterson. (2006). Quantum Chemistry. Elsevier Academic Press. Tercera Edicion.

[36] J. H. Pacheco-Sánchez, M. A. Pacheco-Blas, EMN Meeting on Computation and Theory 2015, Abstract 11-12.

[37] E. Poulain, S. Castillo. *XI Simposio Iberoamericano de Catálisis*. Guanajuato, México. Acta 182 (1988) 1297-1307.

[38] E. Poulain, S. Castillo, A. Cruz, and V. Bertin, *Rev. Mex. Fís.* 41 (1995) 50.

[39] T. Iwasita, J. Braz. Chem. Soc., 13 (2002) 401.

[40] K. Míšek, Czechoslovak Journal of Physics 29 (1979) 1243.

[41] J. J. Jackson, Lattice Defects in Quenched Metals, Academic, New York, (1965), p 467, 479.

[42] Perdew, J. P., Wang. Y. Phys. Rev. B., 45, (1992) 13244.

[43] Perdew, J. P., Wang. Y. Phys. Rev. B., 33, (1986) 8800.

[44] NIST Data Gateway. Available on internet.

[45] Atkins, P., Paula, J. 2010. Physical Chemistry. W. H. Freeman and Company, Novena Edición. New York.

[46] C. W. Oatley, *Proceedings of the Physical Society* 51 (1939) 318.

[47] R. J. Galagali, *Brit. J. Appl. Phys.* 15 (1964) 208.